Internal electric field and photocurrent of polymer/perylene heterojunction solar cell

Ichiro Hiromitsu*, Shin-ichiro Mada, Ayumi Inoue, Yuki Yoshida, and Senku Tanaka[1]

Department of Material Science, Faculty of Science and Engineering, Shimane University, Matsue 690-8504, Japan

[1]*Center for Integrated Research in Science, Shimane University, Matsue 690-8504, Japan*

(Received)

The internal electric field in a heterojunction solar cell made of poly(5-(2'-ethylhexyloxy)-2-methoxy-1,4-phenylenevinylene) (MEH-PPV) as a donor and 3,4,9,10-perylene-tetracarboxyl-bis-benzimidazole (PTCBI) as an acceptor is studied by electroabsorption (EA). The 1ω-EA signal detected at the fundamental electric-field-modulation frequency ω comes from the bulk of the film for MEH-PPV but from the interface of the film for PTCBI. The bias dependence of the bulk electric field for MEH-PPV is correlated with that of the photocurrent generated by MEH-PPV excitation, indicating that the electric field has an essential role in carrier photogeneration. An analysis of the photocurrent action spectrum indicates that the photocurrent-active region in the MEH-PPV layer changes its location depending on the applied bias voltage. This suggests that the region of strong electric field in the MEH-PPV layer changes its location along with the active layer.

* E-mail address: hiromitu@riko.shimane-u.ac.jp

KEYWORDS: solar cells, heterojunction, organic semiconductors, conducting polymers, electroabsorption

1. Introduction

An organic-thin-film solar cell is one of the candidates for practical devices based on organic semiconductors.[1,2] The energy conversion efficiency of the organic cell has been improved to ~ 5%,[3,4] and much effort is being made to improve the efficiency and stability of the organic cell. However, the mechanism of carrier generation in the organic cell has not yet been clearly understood. Generally, the efficiency of the organic cell is enhanced by incorporating donor/acceptor interfaces,[1,2] clearly indicating that the photoinduced electron transfer between a donor and an acceptor is an effective pathway for carrier generation. The efficiency should also be affected by the internal electric field, but no clear picture on the role of the electric field in carrier generation has been obtained.

The carrier-generation mechanism of organic solar cells may be directly related to that of organic thin films in photoconductivity measurement.[5-8] In the latter case, strongly bound Frenkel-type excitons are generated by photoexcitation. Then, weakly bound electron-hole pairs are generated by the dissociation of excitons at donor/acceptor interfaces, organic/metal interfaces, or impurity sites. These bound electron-hole pairs are sometimes called geminate electron-hole pairs or charge transfer excitons. The bound electron-hole pairs further dissociate into free carriers with the aid of electric field. A similar carrier-generation mechanism may occur in organic solar cells. In the case of heterojunction-type solar cells, the bound electron-hole pairs are mainly generated by photoinduced electron transfer at a donor/acceptor interface, and then, the electric-field-assisted dissociation of the pairs into free carriers may occur. However, the role of the electric field has not yet been well demonstrated experimentally. That is why an experimental study of the internal electric field in organic solar cells is important.

Our group has been studying the internal electric field in organic-thin-film solar

cells by electroabsorption (EA). In the EA measurement, an electric-field modulation is applied to the device and a synchronous change in optical-absorption coefficient is detected. 1ω-EA intensity, which is the EA-signal intensity detected at the fundamental modulation frequency ω, is proportional to the internal electric field, so that, by measuring the 1ω-EA intensity, the information about the internal electric field can be obtained.[9] An important aspect of the EA technique is that, when applied to heterojunction cells, the separate observation of the internal fields of the donor and acceptor layers is possible from the 1ω-EA-signal intensities of the two spectral components. By investigating the correlation between the internal field and the photocurrent, we can judge whether the internal field is responsible for carrier generation.

By this method, the role of the internal electric field has been studied for several types of organic solar cell: Schottky-barrier cells made of Zn-phthalocyanine (ZnPc)[10,11] and heterojunction cells using ZnPc as the donor and 3,4,9,10-perylene-tetracarboxyl-bis-benzimidazole (PTCBI)[12] or C_{60}[13] as the acceptor. In most of cases, a good correlation was observed between the internal field and the photocurrent. In particular, the internal field in the ZnPc layer was quenched with a forward bias voltage larger than, typically, 0.5 V, and, simultaneously, the photocurrent produced by ZnPc excitation was quenched.[10,12,13] This clearly indicates that the internal electric field is necessary for free-carrier generation. There were two exceptions in the correlation. The first exception was for a Au/ZnPc/In/Al Schottky barrier cell.[10] In this case, the internal field in the ZnPc layer was quenched with a bias voltage larger than 0.5 V, while the photocurrent produced by ZnPc excitation was not quenched but was increased steeply in this bias region. It was found, however, that the steep increase in photocurrent is not due to an increase in carrier-generation efficiency but to the

enhancement of the carrier transport at the ZnPc/In interface, which was due to the trapping of photogenerated charges in the interface region. The second exception was for a Au/ZnPc/PTCBI/In/Al heterojunction cell.[12] In this case, a good correlation was observed for the ZnPc layer, but no correlation was observed for PTCBI. The absence of the correlation for PTCBI was explained as follows: The internal field of the PTCBI layer detected by EA measurement was the interfacial field at the PTCBI/In junction, while the photocurrent was generated by the bulk electric field in the PTCBI layer. EA was insensitive to the bulk field possibly because the third-order susceptibility of PTCBI, which is proportional to the EA-signal intensity, was very small. The interfacial field at the PTCBI/In junction could be detected by EA, probably because an anomalously large electric field was present at the interface.

In the present paper, the study is extended to a polymer-based heterojunction cell using poly(5-(2'-ethylhexyloxy)-2-methoxy-1,4-phenylenevinylene) (MEH-PPV) as the donor and PTCBI as the acceptor. The molecular structures of MEH-PPV and PTCBI are shown in Fig. 1. A finite electric field is detected in the MEH-PPV layer under the forward bias condition, which is in contrast to the cases of the cells using ZnPc as the donor. As a result, a finite photocurrent produced by MEH-PPV excitation is observed under the forward bias condition. The importance of the electric field in carrier photogeneration is demonstrated.

2. Experimental procedure

2.1 Sample preparation

MEH-PPV was purchased from Aldrich and used without purification. PTCBI was synthesized by a procedure cited in the literature[14)] and used after subliming twice in vacuum. ITO-coated glass plates with a sheet resistance of 50 Ω/sq were purchased

from Geomatec.

The arrangement of the thin films in the heterojunction system is shown in Fig. 2. On an ITO-coated glass substrate, an MEH-PPV film was deposited by spin casting from chloroform solution. Then, PTCBI, In and Al thin films were evaporated at a pressure of 1×10^{-4} Pa. The Al film is a supporting electrode for In because the conductivity of the In film is poor.[15] In/Al was used as a cathode because it had a higher conversion efficiency than the widely used LiF/Al cathode, and also because the devices using In/Al as the top electrode were free from the short-circuit problem in contrast to the devices using Ag as the top electrode. The thickness of the MEH-PPV film was roughly estimated to be ~75 nm from optical absorption intensity. The thicknesses of the PTCBI, In and Al films were determined to be 100, 20 and 30 nm using a quartz oscillator (ULVAC CRTM5000 or CRTM6000) during evaporation. The speeds of the evaporation were 0.1 nm/s for PTCBI, 0.01 nm/s for In and 0.05 nm/s for Al. All measurements were carried out with the sample kept in air at room temperature.

2.2 EA measurement

The internal electric field of the device was studied by electroabsorption (EA) measurement, in which an electric-field modulation $E_{\mathrm{m}}\sin\omega t$ was applied to the device and a synchronous change in optical-absorption coefficient was detected. The change in optical-absorption coefficient, $\Delta\alpha$, has the following relationship with the static internal electric field E_0 in the device.[9]

$$\Delta\alpha \propto \mathrm{Im}\,\chi^{(3)}\left[\left(E_0^2+\frac{E_{\mathrm{m}}^2}{2}\right)+2E_0E_{\mathrm{m}}\sin\omega t-\frac{E_{\mathrm{m}}^2}{2}\cos 2\omega t\right] \qquad (1)$$

Here, $\mathrm{Im}\chi^{(3)}$ is the imaginary part of the third-order electric susceptibility. Equation (1) shows that the amplitude of the 1ω-response at the fundamental frequency ω is

proportional to E_0E_m. Thus, by the lock-in detection of this amplitude, information about the internal electric field E_0 can be obtained. On the other hand, the amplitude of the 2ω-response is proportional to E_m^2.

The electric circuit for EA measurement is shown in Fig. 2. The electric-field modulation was applied to the device using a function generator whose output signal was $V_m \sin\omega t$ with a modulation frequency $\omega/(2\pi)$ of 1 Hz and an amplitude V_m of 0.5, 1.0 or 2.0 V. The probe light normally entered the active area of the device from ITO. The light source was a 100 W halogen lamp followed by a monochromator. The transmitted light intensity T was detected from the Al side using a photomultiplier tube. The change in transmitted light intensity, ΔT, due to the electric-field modulation was measured using a lock-in amplifier with the detection frequency of either 1ω or 2ω. ΔT is related to the changes in the optical-absorption coefficients of MEH-PPV and PTCBI, $\Delta\alpha_1$ and $\Delta\alpha_2$ respectively, by the following equation.

$$-\frac{\Delta T}{T} = d_1 \times \Delta\alpha_1 + d_2 \times \Delta\alpha_2 \qquad (2)$$

Here, d_1 and d_2 are the film thicknesses of ZnPc and PTCBI, respectively.

2.3 Photocurrent measurement

Photocurrent was measured using the same light source as that for EA measurement after turning off the electric-field modulation. The light was chopped at 17 Hz and the photocurrent was detected using a lock-in amplifier. The positive direction of the photocurrent is defined in Fig. 2.

3. Results

3.1 Electroabsorption

Figure 3 shows the 1ω-electroabsorption spectra of the ITO/MEH-PPV/PTCBI/In/Al heterojunction cell for the external bias voltages, V_{bias}, of 2, 0 and –2 V. The spectrum for V_{bias} = 2 V has a peak at 550 nm, while the spectra for V_{bias} = 0 and –2 V have peaks at 480 and 555 nm. Figure 3(c) also shows the first derivative of the optical absorption spectrum of MEH-PPV and the 1ω-EA spectra of PTCBI, the latter being obtained for two types of device studied previously,[12] i.e., a Au/Zn-phthalocyanine(ZnPc)/PTCBI/In/Al heterojunction and a Au/PTCBI/In/Al Schottky junction. First, we make some comments on these PTCBI spectra.

The thin solid curve in Fig. 3(c) shows the 1ω-EA spectrum of Au/ZnPc/PTCBI/In/Al with V_{bias} = 1 V. This spectrum is nearly identical to the first derivative of the absorption spectrum of a PTCBI film and does not contain the ZnPc signal because the internal electric field of ZnPc is quenched under this bias condition.[12] The broken curve in Fig. 3(c) shows the 1ω-EA spectrum of Au/PTCBI/In/Al with V_{bias} = 0 V. These two PTCBI 1ω-EA spectra mainly come from the interface of the PTCBI film because the intensity of these spectra shows a small bias dependence.[12,16] It is observed that the shape of the spectrum for the interfacial PTCBI strongly depends on the device structure.

Now, the 1ω-EA spectrum of the present ITO/MEH-PPV/PTCBI/In/Al cell shown in Fig. 3(c) is compared with the other spectra in Fig. 3(c). It is observed that the peak at 550 nm in the EA spectrum of ITO/MEH-PPV/PTCBI/In/Al is mainly attributed to MEH-PPV, with an overlap of the PTCBI signal, because the first derivative of the absorption spectrum of MEH-PPV has a peak at 550 nm. The broad peak at 480 nm, on the other hand, is attributed to PTCBI with a possible overlap of the MEH-PPV signal.

The features of the present EA spectrum of PTCBI in ITO/MEH-PPV/PTCBI/In/Al are different from those of the PTCBI spectra shown by the thin-solid and broken curves

in Fig. 3(c), particularly in the longer wavelength region of 600 nm < λ < 800 nm, where the present PTCBI spectrum has a very weak signal. An important question is whether the present PTCBI spectrum comes from the bulk or interface of the PTCBI layer. To answer this question, the 2ω-EA spectrum, which is the EA spectrum detected at twice the modulation frequency, was measured. The 2ω-spectrum is known to come from the bulk of the film.[16] Figure 4 shows the 2ω-EA spectrum of the present ITO/MEH-PPV/PTCBI/In/Al cell measured with an increased sensitivity using the modulation amplitude of V_m = 2 V instead of 1 V. The peak of the 2ω-spectrum at 550 nm is attributed to MEH-PPV, and the peaks at 490, 645 and 675 nm are attributed to PTCBI. By comparing the 2ω-spectrum in Fig. 4 with the 1ω-spectrum of the present device in Fig. 3(c), the 1ω-spectrum does not have the peaks at 645 and 675 nm coming from the bulk PTCBI. This indicates that the 1ω-PTCBI spectrum of the present device mainly comes from the interface of the PTCBI layer. Thus, no information on the bulk electric field in the PTCBI layer is obtained from the 1ω-PTCBI spectrum. This situation is similar to that of the previously studied Au/ZnPc/PTCBI/In/Al system.[12] On the other hand, the 1ω-spectrum of MEH-PPV in the present device originates from the bulk of the MEH-PPV layer because it has the same features as the 2ω-MEH-PPV spectrum in Fig. 4 and also its intensity has a good correlation with the photocurrent, as shown in §3.2.

Figure 3(b) shows the 1ω-EA spectrum for V_{bias} = 0 V. This spectrum has the same line shape as that for V_{bias} = –2 V in Fig. 3(c) having a smaller intensity. This indicates that the electric fields in the bulk of the MEH-PPV layer and at the interface of the PTCBI layer are small. For V_{bias} = 2 V, on the other hand, the 1ω-EA spectrum of the present device shows only a peak at 550 nm, as shown in Fig. 3(a). This indicates that the spectrum consists only of the MEH-PPV signal. Since the sign of the peak height at

550 nm is opposite to that for the cases of V_{bias} = 0 and –2 V, the internal field in the MEH-PPV layer is inverted by applying the forward bias of 2 V. On the other hand, the internal field at the PTCBI interface is very small for V_{bias} = 2 V because no PTCBI signal is observed. It is also suggested that the electric field in the bulk of the PTCBI layer is also small for V_{bias} = 2 V, because no trace of the bulk PTCBI signal is observed even in the frequency range of 450 nm < λ < 500 nm, where the bulk PTCBI signal should have a sufficient intensity. It is noted that the PTCBI signal in the 1ω-EA spectrum cannot be observed at $V_{bias} \geq 0.5$ V.

In the present ITO/MEH-PPV/PTCBI/In/Al cell, the EA spectra of MEH-PPV and PTCBI have line shapes near the first derivatives of the absorption spectra, indicating that the excitons generated in the MEH-PPV and PTCBI layers are strongly bound Frenkel-type excitons.[17] In this case, the EA signal intensity is proportional to the change in polarizability upon optical excitation.[17] The present 2ω-EA spectrum of the bulk PTCBI has no signal for 700 nm < λ < 800 nm, while the first derivative of the absorption spectrum of PTCBI has a finite intensity in this wavelength range. It is noted that the EA spectrum of the bulk PTCBI has never been reported. The absence of the signal for 700 nm < λ < 800 nm indicates that the low-energy excitation of the bulk PTCBI does not induce a significant change in polarizability. This might result in a low carrier-photogeneration efficiency, which is shown in §3.2.

3.2 Photocurrent

Figure 5(a) shows the photocurrent action spectra of the ITO/MEH-PPV/PTCBI/In/Al heterojunction cell for V_{bias} = –2, 0, 1, and 2 V with the light incident from the ITO side, and Fig. 5(b) shows the optical absorption spectra of the MEH-PPV and PTCBI films. The action spectrum for V_{bias} = –2 V shows a large

negative photocurrent for 550 nm < λ < 750 nm, which is clearly due to PTCBI excitation, but shows a small photocurrent for 450 nm < λ < 550 nm where MEH-PPV has a strong absorption.

The action spectrum for V_{bias} = –2 V is explained using a model in which the photocurrent-active region is located near the MEH-PPV/PTCBI interface, as shown in Fig. 6(b). In this case, the fraction P_1 of the incident photons absorbed by the active region in the MEH-PPV film is calculated by

$$P_1 = T_{\text{ITO}} \times \exp(-\alpha_1 \times d_1^{\text{inactive}}) \times [1 - \exp(-\alpha_1 \times d_1^{\text{active}})], \quad (3)$$

where T_{ITO} is the transmissivity of the ITO film, which is 0.85 in the visible region, α_1 is the absorption coefficient of the MEH-PPV film, and d_1^{active} and d_1^{inactive} are the thicknesses of the active and inactive regions, respectively, in the MEH-PPV film. Similarly, the fraction P_2 of the photons absorbed by the active region in the PTCBI film is calculated by

$$P_2 = T_{\text{ITO}} \times \exp[-\alpha_1 \times (d_1^{\text{inactive}} + d_1^{\text{active}})] \times [1 - \exp(-\alpha_2 \times d_2^{\text{active}})], \quad (4)$$

where α_2 and d_2^{active} are the absorption coefficient and thickness of the active region, respectively, for the PTCBI film. The incident photon-to-current conversion efficiency (IPCE) is calculated by

$$\text{IPCE} = \Phi_1 \times P_1 + \Phi_2 \times P_2, \quad (5)$$

where Φ_1 and Φ_2 are the quantum efficiencies for the photocurrent generation in the MEH-PPV and PTCBI films, respectively.

The broken line in Fig. 5(a) shows the result of the simulation with d_1^{active} = 30 nm, d_1^{inactive} = 45 nm, d_2^{active} = 30 nm, Φ_1 = 0.09, and Φ_2 = 0.035. The agreement between the experiment and the simulation is satisfactory except for λ > 700 nm. The disagreement for λ > 700 nm may indicate that the quantum efficiency Φ_2 of PTCBI decreases in this

low-energy region. This correlates with the absence of the 2ω-EA signal intensity of the bulk PTCBI in this wavelength region shown in §3.1. The low EA signal intensity is attributed to a small polarizability change by optical excitation, which might result in a low quantum efficiency. The small photocurrent for 450 nm < λ < 550 nm is due to the optical filtering effect by the inactive region in the MEH-PPV film. From the result of the simulation, it is concluded that the photocurrent-active region for $V_{\text{bias}} = -2$ V exists near the MEH-PPV/PTCBI interface. A similar conclusion is obtained for $V_{\text{bias}} = 0$ V. It is noted that, in the simulation, the effects of optical interference and the wavelength dependence of the quantum efficiency were neglected. Thus, the simulation is only qualitative but still can be used to determine the location of the active region.

The action spectrum for $V_{\text{bias}} = 2$ V in Fig. 5, on the other hand, shows a large positive photocurrent for 420 nm < λ < 550 nm, where MEH-PPV has a strong absorption. The shape of the action spectrum in this wavelength range is similar to that of the optical absorption spectrum of MEH-PPV, indicating the absence of the optical filtering effect at $V_{\text{bias}} = 2$ V. A simulation indicates that the photocurrent-active region in the MEH-PPV layer is not located near the MEH-PPV/PTCBI interface but is located near the ITO/MEH-PPV interface, as shown in Fig. 6(a). In this case, the fraction P_1' of the photons absorbed by the active region in the MEH-PPV film is calculated by

$$P_1' = T_{\text{ITO}} \times [1 - \exp(-\alpha_1 \times d_1^{\text{active}})]. \qquad (6)$$

The solid line in Fig. 5(a) shows the result of the simulation with $d_1^{\text{active}} = 10$ nm, $d_1^{\text{inactive}} = 65$ nm, $d_2^{\text{active}} = 30$ nm, $\Phi_1 = 0.05$, and $\Phi_2 = 0.021$. The agreement between the experiment and the simulation is qualitatively reasonable. Thus, it is concluded that the photocurrent-active region in the MEH-PPV layer for $V_{\text{bias}} = 2$ V is located near the ITO/MEH-PPV interface. For PTCBI, on the other hand, it is difficult to determine the

location of the active region because the photocurrent produced by the excitation of PTCBI is small for V_{bias} = 2 V. The above-mentioned simulation was performed by assuming tentatively that the active region in the PTCBI film was located near the MEH-PPV/PTCBI interface.

The photocurrents I_{photo} produced by the excitations of MEH-PPV and PTCBI were measured by illumination at λ = 450 and 650 nm, respectively, because the optical absorption spectra of the two organic species had a very small mutual overlap at these wavelengths. Figure 7 shows the bias dependence of these photocurrents. The I_{photo} produced by the excitation of MEH-PPV has a weak bias dependence for $-2\ V \le V_{bias} \le 0.5\ V$, but increases steeply for $V_{bias} \ge 0.5$ V. The sign of the photocurrent produced by MEH-PPV excitation is different between the two cases of V_{bias} = 2 and –2 V, which correlates with the different signs of the internal field of MEH-PPV for these two bias voltages shown by the present EA result in Fig. 3.

In the case of PTCBI excitation in Fig. 7, I_{photo} again has a weak bias dependence for $-2\ V \le V_{bias} \le 0.5$ V, increases steeply at $0.5\ V < V_{bias} < 0.8$ V, and takes small positive values for $V_{bias} > 0.8$ V. In the present EA result, it was not possible to measure the bulk electric field of the PTCBI layer, but it was suggested that the bulk field of PTCBI is negligibly small for $V_{bias} > 0.5$ V, because no trace of the PTCBI signal was observed in this bias region. This may correlate with the very small photocurrent produced by PTCBI excitation for $V_{bias} > 0.8$ V.

It is interesting to compare the present results with the previous results for a Au/ZnPc/PTCBI/In/Al heterojunction system.[12] In the latter case, the I_{photo} produced by ZnPc excitation disappeared for $V_{bias} > 0.6$ V because the EA-signal intensity, or the internal electric field, of the ZnPc layer disappeared. In the present system, the I_{photo} produced by MEH-PPV excitation had significantly large positive values for $V_{bias} > 1$ V,

which is due to a significantly large positive electric field in the MEH-PPV layer. This comparison further confirms the importance of the electric field in carrier generation.

4. Discussion

In the present results, the internal electric field had a correlation with the photocurrent, indicating that the electric field has an essential role in carrier generation. This suggests that the photocurrent-active region is accompanied by a strong electric field, which was detected by the EA technique. Figure 8 shows the band diagrams proposed on the basis of the present results. For V_{bias} = –2 V, the location of the photocurrent-active region was near the MEH-PPV/PTCBI interface, as shown in Fig. 6(b). This suggests that a strong band bending occurs near the MEH-PPV/PTCBI interface, as shown in Fig. 8(a), and, as a result, a strong electric field is formed in this region. For V_{bias} = 2 V, on the other hand, the location of the photocurrent-active region in the MEH-PPV layer was near the ITO/MEH-PPV interface, as shown in Fig. 6(a). This suggests that a strong band bending occurs near the ITO/MEH-PPV interface, as shown in Fig. 8(b), while the small photocurrent produced by PTCBI excitation suggests a very weak band bending in the PTCBI layer. These band diagrams are in agreement with the present EA results that the sign of the internal field in the MEH-PPV layer is different between the two cases of V_{bias} = –2 and 2 V, and that the internal field in the PTCBI layer is nearly quenched for V_{bias} = 2 V.

The origin of band bending should be the formation of space charges, which is indicated by Poisson's equation. For $V_{bias} \leq 0$ V, negative space charges should be formed in the band bending region of the MEH-PPV layer, and positive space charges in the bending region of the PTCBI layer. Similarly, for V_{bias} = 2 V, negative space charges should be formed in the bending region of the MEH-PPV layer. These space charges

may be the ionized traps, the charges of which may be supplied by the injection from the electrode or by the electron transfer between the two organic layers.

The present results are in agreement with the model of the electric-field-assisted dissociation of bound electron-hole pairs,[5-8] which are generated by photoinduced electron transfer at the donor/acceptor interface, organic/metal interface or impurity sites. For $V_{bias} \leq 0$ V, the electron-hole pairs generated by photoinduced electron transfer at the donor/acceptor interface should be the major precursors for the photoinduced free carriers. For $V_{bias} = 2$ V, on the other hand, the precursors may possibly be the pairs generated by the electron transfer at the organic/metal interface. It is not clear, however, whether the impurity sites contribute to the pair generation, which is directly related to the question whether the pair generation occurs in the bulk or at the exact interface of the organic layer. If the impurity sites distribute in the bulk, the pair generation may occur in the bulk as well as at the interface. The photocurrent-active region has a finite thickness, as shown by the present simulation of the action spectra. However, the thickness of the active region may possibly be determined by the exciton-diffusion length. Thus, the present result does not give an answer to the question whether the pair generation occurs in the bulk.

In the present system, the photocurrent-active region in the MEH-PPV layer was moved from the MEH-PPV/PTCBI interface to the ITO/MEH-PPV interface by applying a forward bias voltage of 2 V. A similar phenomenon was reported by Marks *et al*.[18] for an ITO/PPV/Al cell, in which the location of the active region was moved from the PPV/Al-interface region to the ITO/PPV-interface region by applying a positive bias of 1.5 V. Marks *et al*. considered that their results are due to the mobility of the electrons being lower than that of the holes: Under the short-circuit condition, only the electrons generated near the PPV/Al interface can reach the Al electrode, while, under

the positive bias of 1.5 V, only the electrons generated near the ITO/PPV interface can reach the ITO electrode. A similar mechanism may partially work in the present system. However, the present results clearly demonstrate that carrier generation is mainly controlled by the internal electric field. Thus, the location of the active layer should be determined by the location of a strong electric field.

5. Conclusions

The present EA study indicated that the internal electric field of the MEH-PPV layer in the ITO/MEH-PPV/PTCBI/In/Al heterojunction cell had different signs for $V_{bias} = -2$ and 2 V. This correlates with the bias dependence of the photocurrent produced by MEH-PPV excitation. The bulk electric field of the PTCBI layer, on the other hand, could not be measured for $V_{bias} < 0.5$ V because a large EA signal coming from the interface of the PTCBI layer overlapped with a small EA signal coming from the bulk of PTCBI. For $V_{bias} > 0.5$ V, on the other hand, it was suggested that the bulk electric field of PTCBI is very weak because no trace of the PTCBI signal was detected. This correlates with the very small photocurrent produced by PTCBI excitation for $V_{bias} > 0.8$ V. Thus, the internal electric field in the ITO/MEH-PPV/PTCBI/In/Al heterojunction cell is correlated with the photocurrent, indicating that the electric field has an essential role in carrier photogeneration. The simulation of the photocurrent action spectra indicated that the location of the photocurrent-active region in the MEH-PPV layer depends on the applied bias voltage. It was suggested that the active region is accompanied by a strong internal field.

References

1. H. Spanggaard and F. C. Krebs: Sol. Energy Mater. Sol. Cells **83** (2004)125.
2. J. J. M. Halls and R. H. Friend: in *Clean Electricity from Photovoltaics*, ed. M. D. Archer and R. Hill (Imperial College Press, London, 2001) Chap. 9.
3. W. Ma, C. Yang, X. Gong, K. Lee, and A. J. Heeger: Adv. Funct. Mater. **15** (2005) 1617.
4. J. Y. Kim, S. H. Kim, H. Lee, K. Lee, W. Ma, X. Gong, and A. J. Heeger: Adv. Mater. **18** (2006) 572.
5. M. Pope and C. E. Swenberg: *Electronic Processes in Organic Crystals and Polymers* (Oxford University Press, New York, 1999) 2nd ed., Chap. 13.
6. V. I. Arkhipov and H. Bässler: in *Physics of Organic Semiconductors*, ed. W. Brütting (Wiley-VCH, Weinheim, 2005) Chap. 7.
7. J. Noolandi and K. M. Hong: J. Chem. Phys. **70** (1979) 3230.
8. C. L. Braun: J. Chem. Phys. **80** (1984) 4157.
9. I. H. Campbell, T. W. Hagler, D. L. Smith, and J. P. Ferraris: Phys. Rev. Lett. **76** (1996) 1900.
10. I. Hiromitsu and G. Kinugawa: Jpn. J. Appl. Phys. **44** (2005) 60.
11. I. Hiromitsu, Y. Murakami, and T. Ito: Solid State Commun. **119** (2001) 357.
12. I. Hiromitsu, Y. Murakami, and T. Ito: J. Appl. Phys. **94** (2003) 2434.
13. I. Hiromitsu and G. Kinugawa: Synth. Met. **153** (2005) 73.
14. T. Maki and H. Hashimoto: Bull. Chem. Soc. Jpn. **25** (1952) 411.
15. F.-R. Fan and L. R. Faulkner: J. Chem. Phys. **69** (1978) 3334.
16. P. A. Lane, J. Rostalski, C. Giebeler, S. J. Martin, D. D. C. Bradley, and D. Meissner: Sol. Energy Mater. Solar Cells **63** (2000) 3.
17. L. Sebastian. G. Weiser, and H. Bässler: Chem. Phys. **61** (1981) 125.

18. R. N. Marks, J. J. M. Halls, D. D. C. Bradley, R. H. Friend, and A. B. Holmes: J. Phys.: Condens. Matter **6** (1994) 1379.

Figure captions

Fig. 1. Molecular structures of MEH-PPV and PTCBI.

Fig. 2. Scheme of ITO/MEH-PPV/PTCBI/In/Al heterojunction and electric circuit for EA measurement.

Fig. 3. 1ω-EA spectra of ITO/MEH-PPV/PTCBI/In/Al. (a) V_{bias} = 2 V, (b) 0 V, and (c) −2 V. The frequency $\omega/(2\pi)$ and amplitude V_m of the electric field modulation $V_m \sin\omega t$ are 1 Hz and 1 V, respectively. The thick solid curves in (a) and (c) show the first derivatives of the optical absorption spectrum of an MEH-PPV film. The thin solid curve in (c) shows the 1ω-EA spectrum of PTCBI in a Au(13 nm)/ZnPc(50 nm)/PTCBI(50 nm)/In/Al heterojunction cell with V_{bias} = 1 V. The EA signal of ZnPc in this cell is quenched under this bias condition. The broken curve in (c) shows the 1ω-EA spectrum of PTCBI in a Au(13 nm)/PTCBI(100 nm)/In/Al Schottky junction with V_{bias} = 0 V. The signal intensities of the PTCBI spectra shown by the thin-solid and broken curves are in arbitrary units.

Fig. 4. 2ω-EA spectrum of ITO/MEH-PPV/PTCBI/In/Al with V_{bias} = 0 V. The frequency $\omega/(2\pi)$ and amplitude V_m of the electric field modulation $V_m \sin\omega t$ are 1 Hz and 2 V, respectively. The broken curve shows the 1ω-EA spectrum of PTCBI in a Au(13 nm)/PTCBI(100 nm)/In/Al Schottky junction with V_{bias} = 0 V, the signal intensity of which is in arbitrary units.

Fig. 5. (a) Photocurrent action spectra of ITO/MEH-PPV/PTCBI/In/Al for V_{bias} = 2, 1,

0, and –2 V. The solid and broken curves show the results of simulation for V_{bias} = 2 and –2 V, respectively. (b) Optical absorption spectra of MEH-PPV and PTCBI films.

Fig. 6. Locations of photocurrent-active regions in ITO/MEH-PPV/PTCBI/In/Al for (a) V_{bias} = 2 V and (b) V_{bias} = –2 V. The location of the active region in the PTCBI film for (a) is not clear and was tentatively assumed to be near the MEH-PPV/PTCBI interface in the simulation of the photocurrent action spectrum for V_{bias} = 2 V.

Fig. 7. Bias dependence of photocurrents produced by excitations of MEH-PPV at λ = 450 nm (●) and PTCBI at λ = 650 nm (○). The light source was the same as that for EA measurement, and the light was chopped at 17 Hz. The photocurrent was detected using a lock-in amplifier.

Fig. 8. Proposed band diagrams of ITO/MEH-PPV/PTCBI/In/Al for (a) V_{bias} = –2 V and (b) V_{bias} = 2 V.

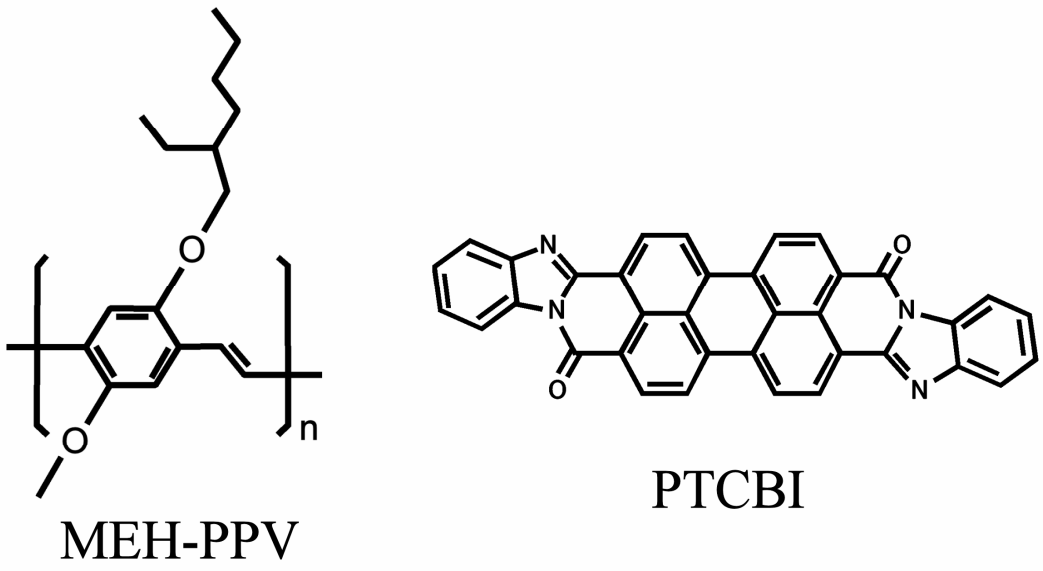

Fig. 1. I. Hiromitsu et al.

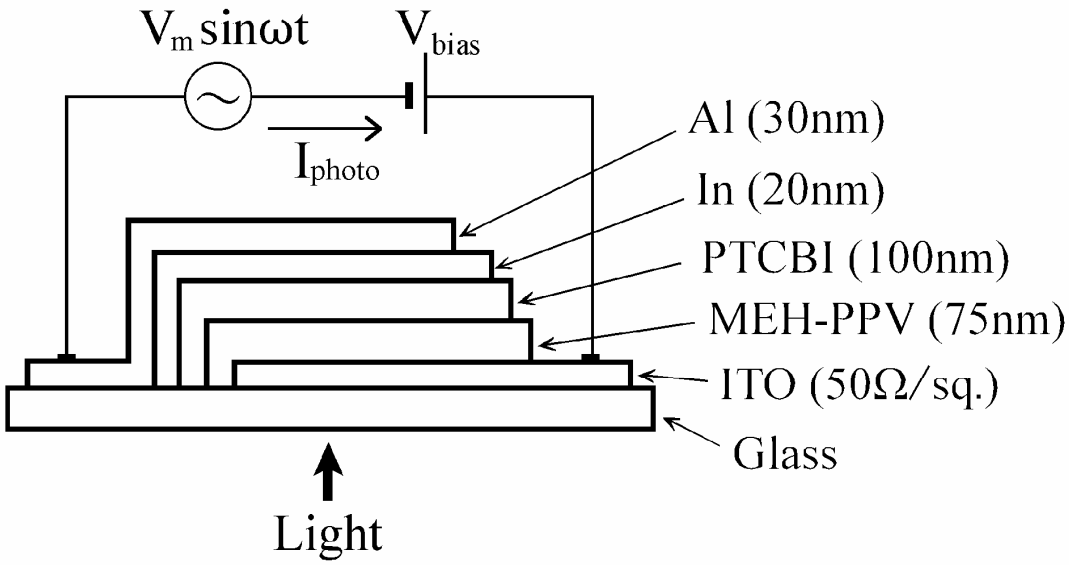

Fig. 2. I. Hiromitsu et al.

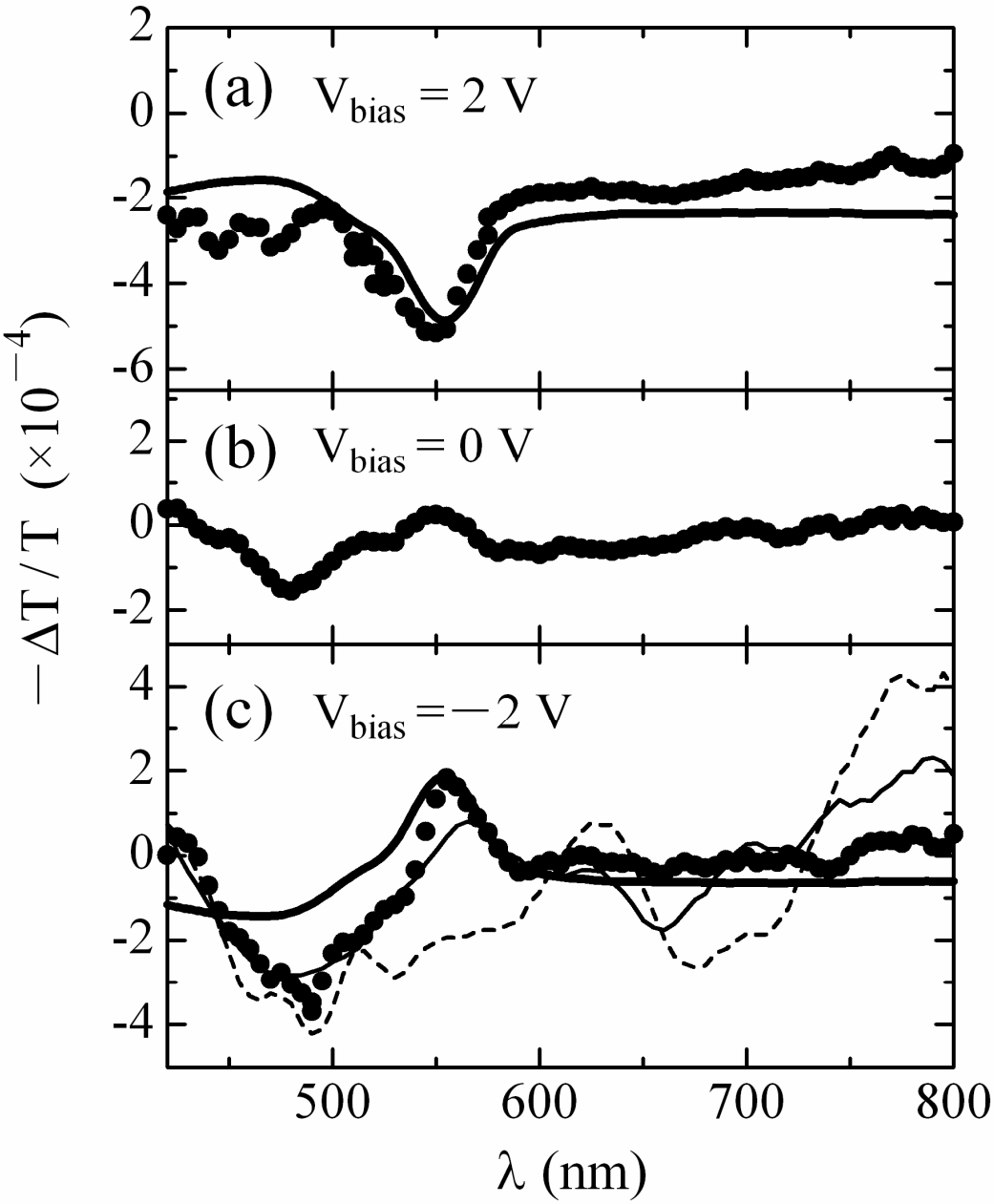

Fig. 3. I. Hiromitsu et al.

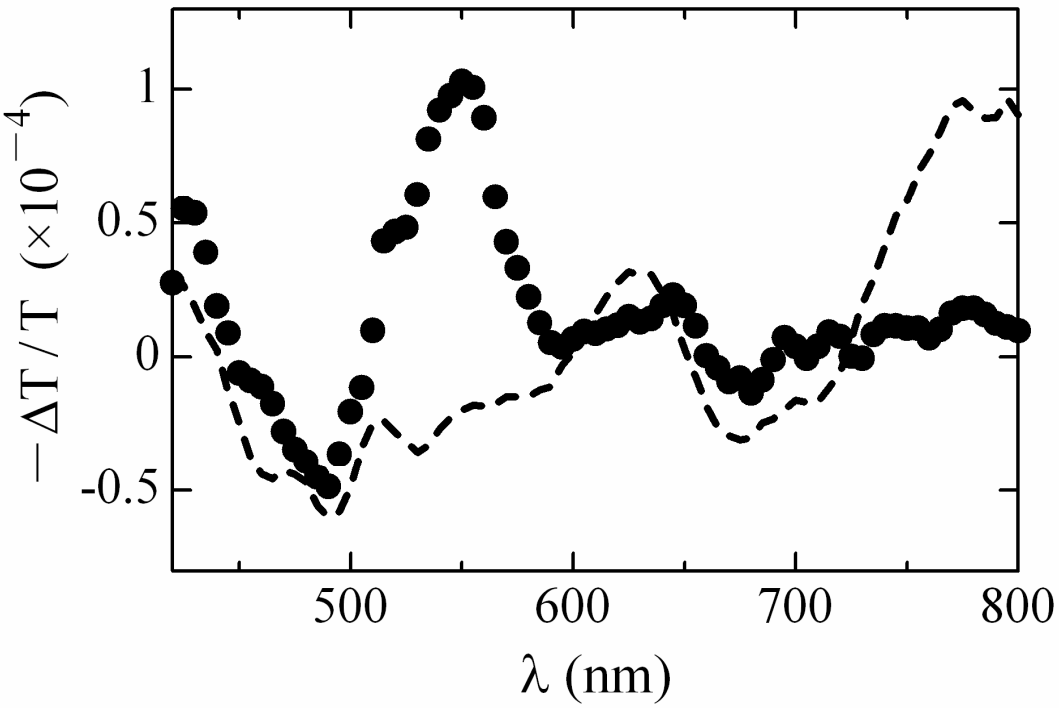

Fig. 4. I. Hiromitsu et al.

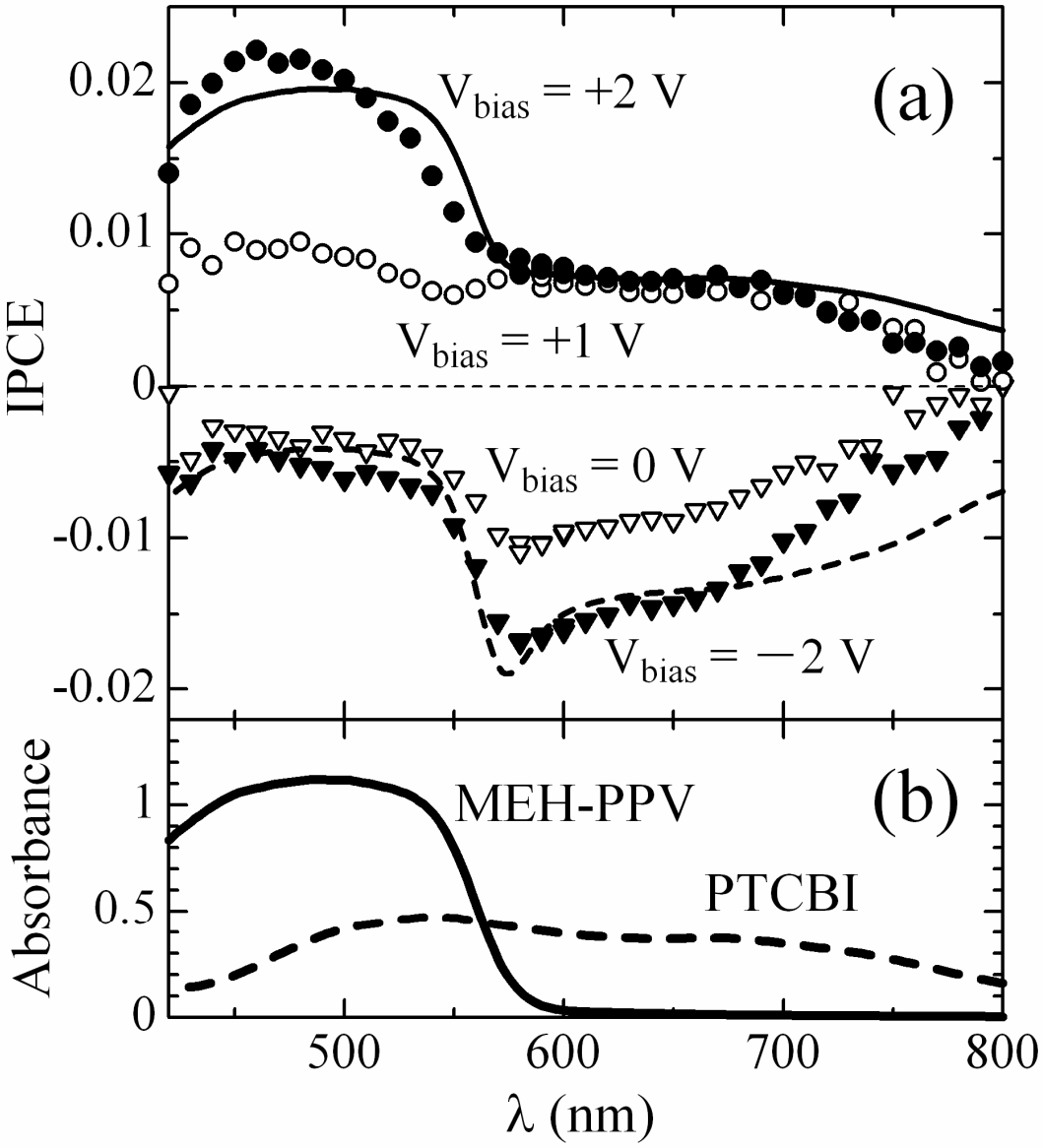

Fig. 5. I. Hiromitsu et al.

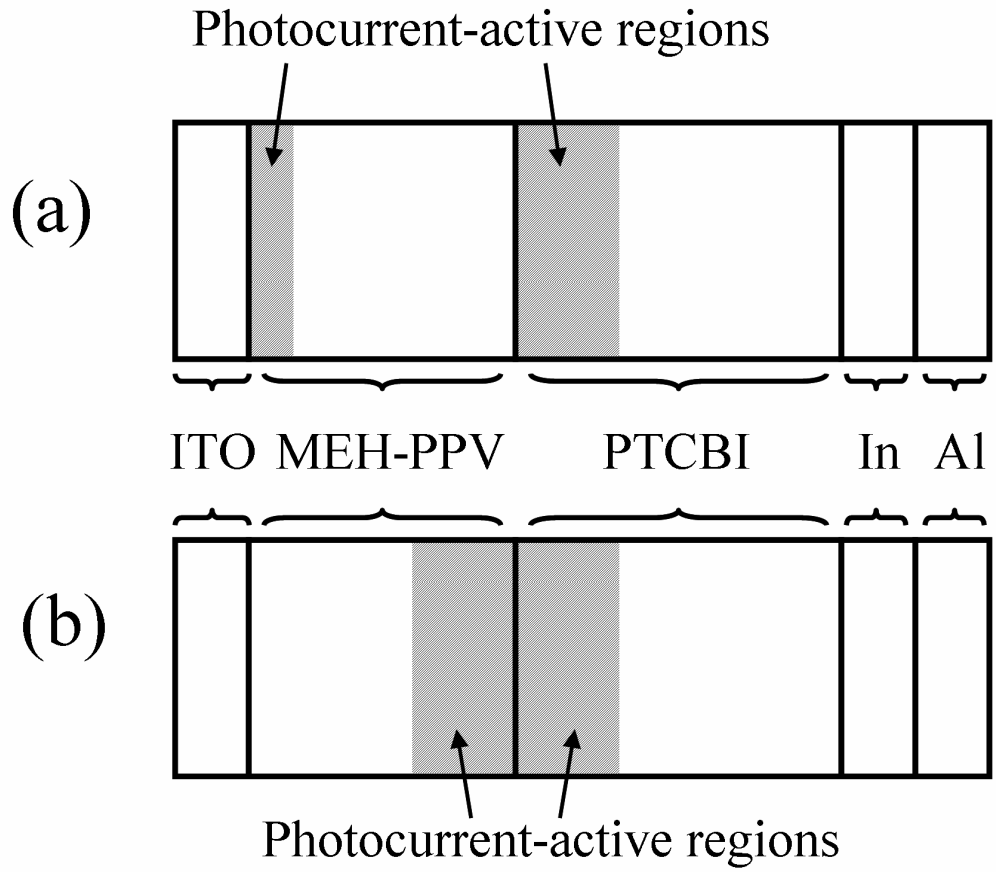

Fig. 6. I. Hiromitsu et al.

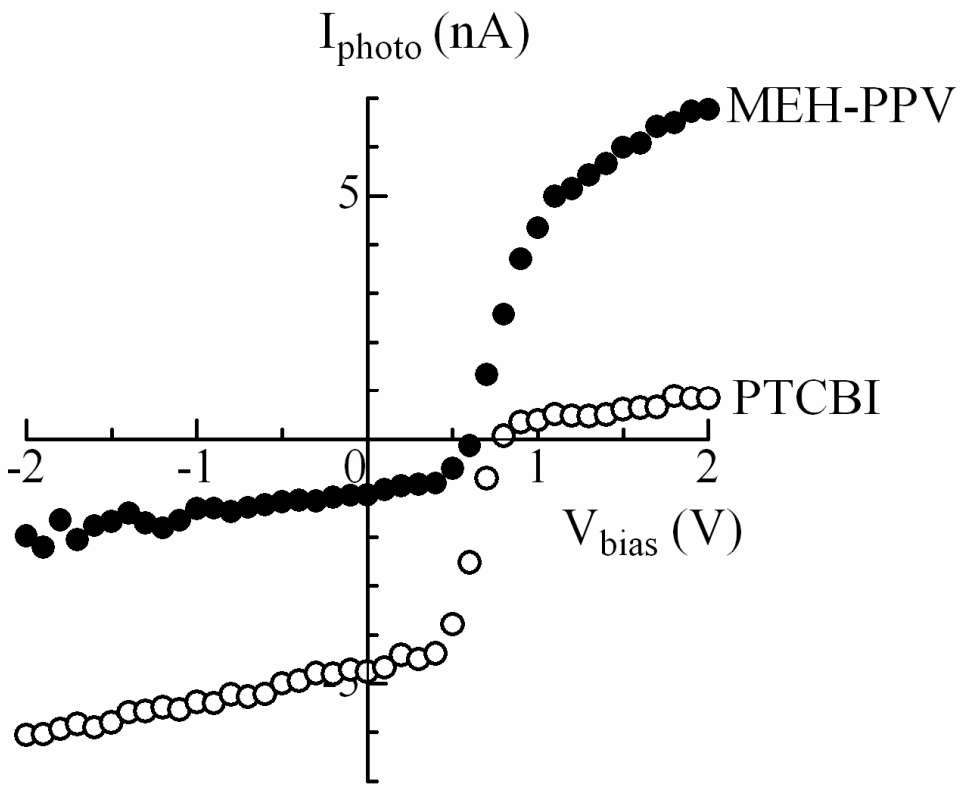

Fig. 7. I. Hiromitsu et al.

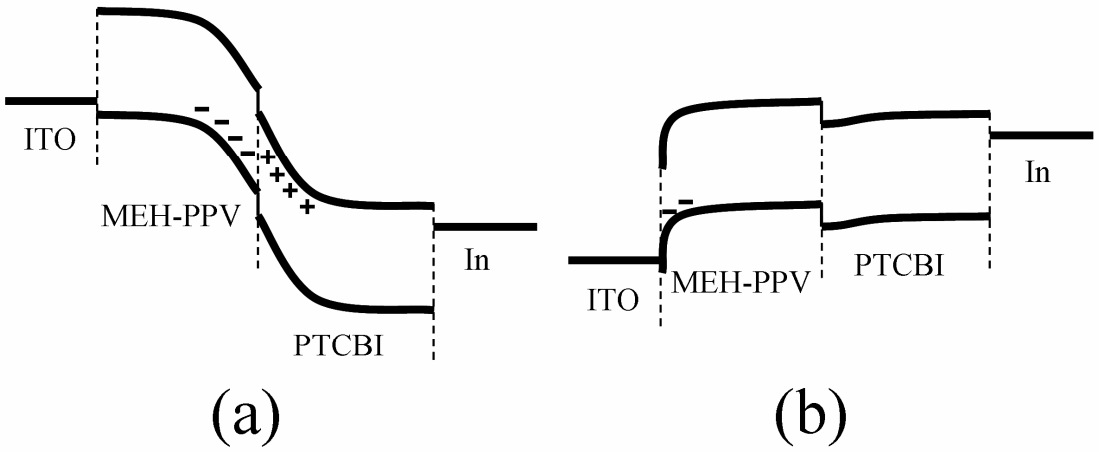

Fig. 8. I. Hiromitsu et al.